Titre: Title:	Quantification of autoignition risk in aeroderivative gas turbine premixers using incompletely stirred reactor and surrogate modeling
Auteurs: Authors:	Salvatore Iavarone, Savvas Gkantonas, Sandeep Jella, Philippe Versailles, Sajjad Yousefian, Rory F. D. Monaghan, Epaminondas Mastorakos, & Gilles Bourque
Date:	2022
Type:	Article de revue / Article
Référence: Citation:	Iavarone, S., Gkantonas, S., Jella, S., Versailles, P., Yousefian, S., Monaghan, R. F. D., Mastorakos, E., & Bourque, G. (2022). Quantification of autoignition risk in aeroderivative gas turbine premixers using incompletely stirred reactor and surrogate modeling. Journal of Engineering for Gas Turbines and Power, 144(12), GTP-22-130 (11 pages). https://doi.org/10.1115/1.4055481

Titre de la revue: Journal Title:	Journal of Engineering for Gas Turbines and Power (vol. 144, no. 12)
Maison d'édition: Publisher:	ASME International
URL officiel: Official URL:	https://doi.org/10.1115/1.4055481
Mention légale: Legal notice:	

Salvatore Iavarone[1]
Department of Engineering,
University of Cambridge,
Trumpington Street,
Cambridge CB2 1PZ, UK;
École polytechnique de Bruxelles,
Aero-Thermo-Mechanics Laboratory,
Université Libre de Bruxelles,
Avenue F. D. Roosevelt 50,
Brussels 1050, Belgium
e-mail: si339@cam.ac.uk

Savvas Gkantonas
Department of Engineering,
University of Cambridge,
Trumpington Street,
Cambridge CB2 1PZ, UK

Sandeep Jella
Siemens Energy Canada Ltd,
9545 Côte-de-Liesse Road,
Montréal, QC H9P 1A5, Canada

Philippe Versailles
Siemens Energy Canada Ltd,
9545 Côte-de-Liesse Road,
Montréal, QC H9P 1A5, Canada

Sajjad Yousefian
Combustion Chemistry Centre,
National University of Ireland,
University Road,
Galway H91 TK33, Ireland

Rory F. D. Monaghan
Combustion Chemistry Centre,
National University of Ireland,
University Road,
Galway H91 TK33, Ireland

Epaminondas Mastorakos
Department of Engineering,
University of Cambridge,
Trumpington Street,
Cambridge CB2 1PZ, UK

Gilles Bourque
Siemens Energy Canada Ltd,
9545 Côte-de-Liesse Road,
Montréal, QC H9P 1A5, Canada

Quantification of Autoignition Risk in Aeroderivative Gas Turbine Premixers Using Incompletely Stirred Reactor and Surrogate Modeling

The design and operation of premixers for gas turbines must deal with the possibility of relatively rare events causing dangerous autoignition (AI). Rare AI events may occur in the presence of fluctuations of operational parameters, such as temperature and fuel composition, and must be understood and predicted. This work presents a methodology based on incompletely stirred reactor (ISR) and surrogate modeling to increase efficiency and feasibility in premixer design optimization for rare events. For a representative premixer, a space-filling design is used to sample the variability of three influential operational parameters. An ISR is reconstructed and solved in a postprocessing fashion for each sample, leveraging a well-resolved computational fluid dynamics solution of the non-reacting flow inside the premixer. Via detailed chemistry and reduced computational costs, ISR tracks the evolution of AI precursors and temperature conditioned on a mixture fraction. Accurate surrogate models are then trained for selected AI metrics on all ISR samples. The final quantification of the AI probability is achieved by querying the surrogate models via Monte Carlo sampling of the random parameters. The approach is fast and reliable so that user-controllable, independent variables can be optimized to maximize system performance while observing a constraint on the allowable probability of AI.
[DOI: 10.1115/1.4055481]

1 Introduction

In typical gas turbines aiming to achieve lean premixed combustion, the design and operation of premixers focus on attaining residence times low enough to prevent autoignition (AI), but high enough to obtain adequate mixing. Premixers are designed to achieve residence time distributions that are at least two orders of magnitude below typical ignition delays [1]. However, at engine conditions, intermediate radicals are formed even at these short time scales and if their reactions can progress to a critical point determined by local mixture concentration, residence time, temperature, and turbulent mixing rates, ignition kernels with localized heat release can form and rapidly lead to a propagating flame in the premixer [2,3]. Thus, rare AI events may occur in the presence of fluctuations of various physical quantities and must be understood and predicted.

Computational fluid dynamics (CFD) simulations can be employed to improve the understanding of the AI process inside a premixer. These simulations must feature an accurate description of the turbulent mixing process and a detailed chemical mechanism that can properly model reaction pathways of low-temperature precursors (e.g., H_2O_2) at high pressures [4].

[1]Corresponding author.
Manuscript received July 11, 2022; final manuscript received July 21, 2022; published online October 4, 2022. Editor: Jerzy T. Sawicki.

However, a significant number of simulations at different operating conditions may be required to design premixers and compute the probability of rare AI events. AI may be caused by the variability of the initial operating conditions of the premixer, and a strategy to compute its probability is to sample a large number of conditions from the distribution that defines their uncertainty, propagate the system in time, and count the number of samples leading to AI. This procedure is carried out by so-called *forward* uncertainty quantification approaches, which determine the uncertainty in the prediction of selected quantities of interest due to known variability of input and/or model parameters, usually described by probability density functions. In combustion studies, forward propagation of uncertainties provided prediction intervals on laminar flame speeds [5,6], ignition delay times [7,8], and NO_X emissions [9–11]. Monte Carlo methods provide the most direct approach for propagating uncertainties and estimating the variability in the predictions, although they require a significant number of realizations. Thus, Monte Carlo methods are unfeasible when the realizations are obtained by CFD simulations due to their high dimensionality and computational cost. Several studies focused on solving these issues by either reducing the number of samples needed to accurately compute the output probability density functions [12–14] or using surrogate models (also known as metamodels) [15–18], which are low-order functions constructed (trained) upon a reduced number of CFD simulations. In the latter case, the training of accurate surrogate models may be still hindered by the high dimensionality of the uncertain parameter space and the computational cost of the several CFD simulations needed. Thus, a crucial need exists to develop and employ computationally inexpensive methods that simplify calculations with detailed turbulence and chemistry models, provide predictions within a reasonable degree of accuracy, and capture system responses to perturbations and, eventually, rare events.

This work presents a methodology based on incompletely stirred reactor (ISR) and surrogate modeling to quantify AI risk in aero-derivative gas turbine premixers accurately and with low computational costs. The ISR modeling removes the need to perform many computationally expensive reacting flow simulations by relying only on one well-resolved CFD simulation of the inert flow, which is then kinetically postprocessed. A surrogate model, trained on several ISR simulations of a premixer, then aims to compute the probability of AI kernel formation and thus quantify the AI risk in the premixer due to the variability of its operational parameters. An ISR can be defined here as the premixer volume within which conditional averages of reacting scalars, conditioned on a mixture fraction that denotes fuel/air mixing, are homogeneous but with the flow and mixture fraction being inhomogeneous. By directly considering the mixing field, provided by a CFD computation and featuring the mixture fraction mean and variance, and the scalar dissipation rate (SDR), ISR equations are solved for reacting scalars, such as concentrations of AI precursors and temperature, so that AI metrics can be explicitly analyzed and used in a surrogate model. This approach is computationally not expensive since the ISR only involves the solution of a set of ordinary differential equations that are solved in a postprocessing fashion, further allowing the use of detailed chemistry. The coupling of CFD with an ISR as a postprocessing step is similar to what is typically performed in Chemical Reactor Network approaches using ideal reactors (e.g., see Ref. [19] for a review). However, an ISR allows for an elaborate treatment of unmixedness and micromixing effects which are crucial for AI and other low Damköhler number phenomena. The ISR theory was first developed by Bilger and coworkers [20–23] on the theoretical foundation laid by the conditional moment closure (CMC) method for turbulent reacting flows [24]. Methods based on ISRs have previously been applied to experimental lab-scale combustors [22,25], a heavy-duty diesel engine [26], and model aero-engine combustors [27–30], demonstrating good accuracy for predicting gas-phase pollutants and soot. More recently, ISR theory has also been validated as a suitable approach to estimate AI propensity. Using a network of ISRs to postprocess non-reacting CFD computations, Iavarone et al. [31,32] successfully reproduced hydrogen AI locations in a turbulent atmospheric coflow of heated air [3], whereas Gkantonas et al. [33] observed the good performance of the ISR network (ISRN) in capturing the AI behavior inside an aero-derivative gas turbine premixer previously studied with reacting CFD [1]. The same premixer used in Refs. [1,33] is also investigated here. However, this work focuses on predicting the occurrence of AI in the premixer, rather than the location of AI kernels. For this purpose, a single ISR, rather than a network, is used, enabling stochastic AI modeling thanks to its reduced computational cost.

The specific objectives of the present work are to (i) perform stochastic AI modeling by considering uncertainties in three influential input quantities, i.e., fuel temperature, air temperature, and fuel mixture composition, of an ISR representation of a premixer with real-life geometric complexity; (ii) investigate the effect of these quantities on the probability of AI; (iii) quantify the AI risk in the premixer at different operating conditions. The first objective of the work is carried out by training a surrogate model on several ISR simulations of the premixer. The ISR simulations are performed in postprocessing and take as input the mixing field, provided by a non-reacting CFD simulation of the premixer, and different possible values of the three influential operating conditions. Temperature and species mass fractions, conditioned on the mixture fraction, are obtained as output and provide indications about the occurrence of AI in the premixer at the considered conditions. For a selected ISR output, which acts as an AI metric, the most accurate response surface, indicating the relationship between the variable and the input parameters, is found by employing and comparing different surrogate-modeling approaches. The second and third objectives are then achieved by querying the surrogate model via Monte Carlo sampling of the random influential input parameters. The paper is structured as follows. The derivation of the ISR equations is first presented, followed by details on the submodels used in the computations. A brief description of the investigated premixer and the mixing field obtained by a reference CFD simulation is then reported. Next, the solution strategy employed for the stochastic modeling of the premixer is presented. Results and key conclusions close the paper.

2 The Incompletely Stirred Reactor Approach

The derivation of the governing equations for an ISR, either as a single reactor or as part of a reactor network, is based on the singly-conditioned CMC method presented in various works (e.g., see Refs. [24,30]) and validated for AI in several studies [34–37]. The ISR equation may be viewed as a zero-dimensional (or spatially integrated) approximation of the full multidimensional CMC equation. The underlying concept is to make the mixture fraction PDF and the SDR, dictating micromixing, appear in the governing equation and consequently extract those quantities from a reference CFD simulation, here describing the non-reacting flow. The ISR equations are solved in a postprocessing fashion so that any chemical mechanism of arbitrary complexity can be used as well as various operating conditions, as considered in Sec. 4 for three influential input parameters. As the flow and mixing fields are precalculated and only a subset of processes are solved, the computational time is drastically reduced compared to a detailed CFD simulation. For the problem of AI, where only small density changes are expected to occur before AI happens, postprocessing non-reacting flow mixing patterns introduces only small errors [4].

2.1 Mathematical Model. An ISR is considered to be a volume V (here, the whole premixer volume) within which conditional averages of reacting scalars, conditioned on the mixture fraction, are independent of position. In contrast to a perfectly-stirred reactor, which has a uniform composition, this allows an ISR to have mixture fraction inhomogeneities which are important for AI calculations. The partially stirred reactor (PaSR) model,

derived from the Monte Carlo PDF method (e.g., see Ref. [38]), has similarities with the ISR model. However, in a PaSR, there is no direct link between the reactor mixing rates and the ones from the flow field. Various versions of the ISR governing equations have appeared in the literature [20–23,26,29]. Here, the derivation is presented for completeness.

The equations are derived from the transport equation of the conditional expectation (here considered to be density-weighted and time-averaged) of a generic species α, $Q_\alpha \equiv \langle Y_\alpha | \xi = \eta \rangle$, but also include the mixture fraction PDF, P_η, with η being the sample space variable of the mixture fraction, ξ. Based on Ref. [24], the transport equation reads

$$\frac{\partial \bar{\rho} Q_\alpha P_\eta}{\partial t} + \frac{\partial}{\partial x_i}\left(\bar{\rho}\langle u_i Y_\alpha | \eta \rangle P_\eta\right) = -Q_\alpha \frac{\partial^2 \bar{\rho}\langle N|\eta\rangle P_\eta}{\partial \eta^2} + \bar{\rho}\langle N|\eta\rangle P_\eta \frac{\partial^2 Q_\alpha}{\partial \eta^2} + \bar{\rho}\langle \dot{\omega}_\alpha | \eta \rangle P_\eta \quad (1)$$

where $N \equiv D \nabla\xi \cdot \nabla\xi$ is the SDR. Note that differential diffusion effects can be included in Eq. (1) but a unity Lewis number assumption is used here instead since no highly diffusive species are present in the fuel-air mixture (see Sec. 3). Considering statistically stationary flow, integration of Eq. (1) over the reactor's volume and the application of the flux divergence theorem to its left-hand side lead to

$$\oint_A \bar{\rho}\langle \mathbf{u}|\eta\rangle Q_\alpha P_\eta \cdot d\mathbf{A} = -\int_V \left(Q_\alpha \frac{\partial^2 \bar{\rho}\langle N|\eta\rangle P_\eta}{\partial \eta^2}\right) dV + \int_V \left(\bar{\rho}\langle N|\eta\rangle P_\eta \frac{\partial^2 Q_\alpha}{\partial \eta^2} + \bar{\rho}\langle \dot{\omega}_\alpha|\eta\rangle P_\eta\right) dV \quad (2)$$

In Eq. (2), conditional correlations between reacting scalars and velocity are neglected, so all fluctuations about the conditional mean in the inlet and outlet flows are not considered, consistent with ISR theory [24]. By definition, conditional reactive scalar statistics and their functions, e.g., chemical source terms, are also considered uniform inside an ISR core. Hence, they can be moved out of the integral on the right-hand side of Eq. (2). This allows for the introduction of the core-averaged mass density, ρ^{**}, mixture fraction PDF, P_η^{**}, and SDR, N_η^{**}, in the equation, which can be computed by CFD simulations after appropriate time-averaging. The core-averaged quantities are given by

$$\rho^{**} \equiv \frac{\int_V \bar{\rho} dV'}{V}; \quad P_\eta^{**} \equiv \frac{\int_V \bar{\rho} P_\eta dV'}{\rho^{**} V}; \quad N_\eta^{**} \equiv \frac{\int_V \bar{\rho}\langle N|\eta\rangle P_\eta dV'}{\rho^{**} V P_\eta^{**}} \quad (3)$$

In addition, a mass-flow-rate-weighted mixture fraction PDF for the inlet and outlet streams can be introduced, which is given by

$$P_\eta^* \equiv \frac{1}{\dot{m}} \int_A \bar{\rho}\langle \mathbf{u}|\eta\rangle P_\eta \cdot d\mathbf{A} \quad (4)$$

Combining Eqs. (2)–(4), the ISR equation then reads

$$\frac{(Q_\alpha P^*)_{\text{out}} - (Q_\alpha P^*)_{\text{in}}}{\tau_r} = -Q_\alpha \frac{d^2 N_\eta^{**} P_\eta^{**}}{d\eta^2} + P_\eta^{**}\left(N_\eta^{**}\frac{d^2 Q_\alpha}{d\eta^2} + \langle \dot{\omega}_\alpha|\eta\rangle\right) \quad (5)$$

where the reactor residence time, $\tau_r \equiv (\rho^{**} V)/\dot{m}$, has been utilized. Note that the partial derivatives in Eq. (2) have been replaced with ordinary ones in Eq. (5) since conditional statistics are now only a function of the mixture fraction. To close the first term on the right-hand side of Eq. (5), the transport equation for the mixture fraction PDF may be utilized [24]. If molecular fluxes are neglected, the PDF equation is equivalent to Eq. (1) with $Q_\alpha = 1$ and no chemistry source term. Since Q_α is constant, its derivative is zero. Considering stationary flow, the integration of the PDF equation over the core volume reads

$$\frac{\oint_A \bar{\rho}\langle \mathbf{u}|\eta\rangle P_\eta \cdot d\mathbf{A}}{\rho^{**} V} = \frac{(P_\eta^*)_{\text{out}} - (P_\eta^*)_{\text{in}}}{\tau_r} = -\frac{d^2 N_\eta^{**} P_\eta^{**}}{d\eta^2} \quad (6)$$

where Eq. (3) and the flux divergence theorem have been applied. Furthermore, to derive the final ISR equation, the conditional averages at the ISR outlet are considered equal to the conditional averages at the core, i.e., $(Q_\alpha)_{\text{out}} = Q_\alpha$, consistent with the stirred reactor concept, as discussed in Ref. [23]. Consequently, the ISR equation may be derived as follows:

$$\frac{(P_\eta^*)_{\text{in}}}{\tau_r P_\eta^{**}}\left(Q_\alpha - (Q_\alpha)_{\text{in}}\right) = N_\eta^{**}\frac{d^2 Q_\alpha}{d\eta^2} + \langle \dot{\omega}_\alpha|\eta\rangle \quad (7)$$

In the special case of completely unmixed inlet streams, as in a premixer, the inlet PDF, $(P_\eta^*)_{\text{in}}$, is zero at $0 < \eta < 1$ since only mixture fractions at 0 or 1 are possible, i.e., the inlet PDF consists of two Dirac δ-functions at the mixture fraction space bounds. Considering that Dirichlet conditions are used for the bounds in CMC and ISR equations, then the ISR equation is written as

$$0 = N_\eta^{**}\frac{d^2 Q_\alpha}{d\eta^2} + \langle \dot{\omega}_\alpha|\eta\rangle \quad (8)$$

Equation (8) is virtually identical to the steady-state flamelet model for unity Lewis number [39]. Although the core-averaged PDF and residence time do not appear in Eq. (8) directly, they dictate the profile of the core-averaged SDR profile, N_η^{**}. The latter may be calculated from the double integral of Eq. (6) as follows:

$$N_\eta^{**} = \frac{1}{\tau_r P_\eta^{**}} \int_0^\eta \int_0^{\eta'} \left((P_{\eta''}^*)_{\text{in}} - (P_{\eta''}^*)_{\text{out}}\right) d\eta' d\eta'' \overset{\text{for Eq. 8}}{=} \frac{1}{\tau_r P_\eta^{**}}\left((1-\bar{\xi})\eta - \int_0^\eta \int_0^{\eta'} (P_{\eta''}^*)_{\text{out}} d\eta' d\eta''\right) \quad (9)$$

where $\bar{\xi}$ is the well-mixed mixture fraction calculated from the mass flow rates of the inlet streams. For example, consider a fuel stream with mass flow rate $\dot{m}_{\text{f}}$ and an oxidizer stream with $\dot{m}_{\text{ox}}$, then $\bar{\xi} = 1/(1 + \dot{m}_{\text{ox}}/\dot{m}_{\text{f}})$.

2.2 Solution Strategy. The ISR approach for AI risk quantification starts with the calculation of the average non-reacting flow field using CFD. As discussed in Ref. [29], the modeling approach for the reference CFD simulation can vary given the availability of resources, but care must be taken for each specific application so that the underlying mixing field is well captured. It is important to note that flame growth and stabilization are not of particular interest from a risk assessment and rare event identification perspective. Consequently, flame effects on the mixing field do not need to be considered in the approach, similar to what was attempted in Refs. [31–33]. In addition, perturbations to influential variables, such as fuel composition and temperature at the premixer inlet, do not affect the inert flow significantly but can alter AI behavior. Thus, non-reacting CFD can be reliably used to describe mixing and then coupled with an ISR for performing sensitivity analyses within a relatively wide range of conditions (concerning AI propensity) and for training a surrogate model. The ISR equations are then solved using an in-house code. Here the form of Eq. (8) is selected since the focus is on aero-derivative premixers with completely unmixed inlet streams. The evaluation of the core-averaged SDR via Eq. (9) requires knowledge of the

mean residence time and the mixture fraction PDF. In this work, these quantities are extracted from a non-reacting CFD simulation, described in detail later. The core-averaged density and mixture fraction PDF are found using Eq. (3) for which some information on the CFD grid is required. At each CFD cell, P_η is modeled with a presumed β-function computed from the time-averaged mixture fraction and the mixture fraction variance, which are readily available from the simulation. In the case of singularities, the β-function is replaced or complemented by δ-functions. In Eq. (9), it is evident that the division with the core-averaged PDF can lead to numerical problems when the PDF tends to zero. To ensure that the SDR does not take unrealistically high values, the division with the PDF can be approximated as $1/P_\eta^{**} \approx P_\eta^{**}/(P_\eta^{**2} + \epsilon^2)$, where ϵ is an absolute tolerance for the core-averaged PDF (here $\epsilon = 10^{-9}$). The double integration in Eq. (9) can also prove cumbersome and may result in negative values of the SDR due to machine precision errors when the PDF tends to zero [24]. The realisability problem could be solved using the methods of [40,41] to find the double integrals numerically without limitations to the PDF shape. However, this might not prove necessary in a premixer system with completely unmixed streams. Assuming that the outlet PDF follows a narrow normal distribution in mixture fraction space around the well-mixed value, i.e., $(P_\eta^*)_{\text{out}} \to \mathcal{N}(\bar{\xi}, \sigma_o^2)$, the double integral can be found analytically using

$$\int_0^\eta \int_0^{\eta''} (P^*_{\eta'\eta''})_{\text{out}}\, d\eta' d\eta'' = \frac{1}{2}\left((\eta - \bar{\xi})\left(1 + \text{erf}\left(\frac{\eta - \bar{\xi}}{\sqrt{2\sigma_o^2}}\right)\right) + \sqrt{\frac{2\sigma_o^2}{\pi}} \exp\left(-\frac{(\eta - \bar{\xi})^2}{2\sigma_o^2}\right)\right) \tag{10}$$

Equation (10) is used to calculate the double integral of the outlet mixture fraction PDF after finding an appropriate standard deviation matching the CFD simulation. Interestingly, in the limit of $\sigma_o \to 0$, i.e., perfect mixing at the outlet, it follows that $(P_\eta^*)_{\text{out}} \to \delta(\eta - \bar{\xi})$, and its double integral is given by $(\eta - \bar{\xi})\mathcal{H}(\eta - \bar{\xi})$ where $\mathcal{H}$ is the Heaviside function. As mentioned previously, the outlet PDF can also be numerically integrated if care is taken to locations of negligible probability [41]. Hence, there is no limitation in the configurations that can be represented. For a scalar ϕ with a conditional mean Q_ϕ, the unconditional mean counterpart within the premixer core and at the outlet can then be found by

$$\phi^{**} = \int_0^1 Q_\phi P_\eta^{**}\, d\eta; \quad \phi^*_{\text{out}} = \int_0^1 Q_\phi (P_\eta^*)_{\text{out}}\, d\eta \tag{11}$$

As far as the numerical setup of the ISR equations is concerned, the mixture fraction space is discretized using 101 nodes clustered around the stoichiometric mixture fraction and sufficient resolution around the most-reactive mixture fraction [4], which will be described later. Pure air is imposed at $\eta = 0$, whereas the fuel composition is imposed at $\eta = 1$. The oxidizer, T_{ox}, and fuel temperature, T_f, are also imposed at the boundaries $\eta = 0$ and $\eta = 1$, respectively. The pressure is assumed constant and equal to the nominal operating pressure of the premixer. The system is assumed adiabatic; therefore, the conditional enthalpy remains constant throughout computations and the conditional temperature may be identified via a reverse calculation (here with an absolute tolerance of 10^{-8}). All simulations are initialized from "pure mixing" solutions using the same boundary conditions. As will be detailed later, the fuel composition, T_{ox} and T_f, and their uncertainty are studied in detail in this paper since they are crucial for AI. An operator splitting technique is then implemented for the solution of the ISR equations, which are marched in time until convergence is reached. First, the diffusion term of Eq. (8) is computed using a second-order accurate numerical scheme and the VODPK solver [42], followed by the integration of the chemistry employing the chemical mechanism by Jella et al. [1] and first-order moment closure [24]. The effect of the operator splitting between diffusion and chemistry has been assessed at steady-state with an amplitude mapping closure model [43] for the conditional SDR profile. The results were then compared with the method of lines finding negligible differences for temperature, major species, and radicals for pseudo-time steps below 2 μs (e.g., see Ref. [44] for a similar assessment applied to the elliptic CMC equation). A constant time-step of 1 μs is used here.

3 Investigated Premixer and Computational Fluid Dynamics Analysis

An experimental premixer is investigated here to demonstrate the ISR stochastic analysis framework. The same premixer was previously studied by Jella et al. using reacting CFD [1]. Furthermore, Gkantonas et al. [33] successfully employed ISR theory to estimate AI propensity in this premixer, so it was preferred here as a benchmark case. The premixer was designed to have a characteristic residence time approximately six times shorter than the worst-case AI delay of typical natural gas and features multiple jets injecting pure air into a cross stream of gaseous fuel in the form of a film [1]. The distributed injection of air and fuel results in a range of residence times that significantly damps Intermediate Frequency Dynamics for a wide range of operating conditions [45].

A representation of the mean flow and mixing fields obtained with non-reacting large eddy simulation (LES) is shown in Fig. 1. The Favre-filtered continuity and momentum equations, as well as transport equations for the mixture fraction, $\tilde{\xi}$, and its subgrid scale variance, $\tilde{\xi''^2}$, were solved using the Star-CCM+ CFD software. The Wall-Adaptive Large Eddy Simulation (WALE) model of Nicoud and Ducros [46] was used to model subgrid stresses. The filtered SDR, $\tilde{N}$, used in the subgrid scale variance transport equation, was computed considering both the resolved and subgrid scale contributions [47,48] as in $\tilde{N} = D\nabla\tilde{\xi}\cdot\nabla\tilde{\xi} + C_N\tilde{\xi''^2}\mu_{\text{sgs}}/(2\rho\Delta^2)$, where $C_N = 42$ [49,50], μ_{sgs} is the subgrid scale viscosity and Δ is the filter width estimated as the cube root of the LES cell volume. The molecular diffusivity was calculated from the kinematic viscosity of the mixture using a constant Schmidt number ($Sc = 0.7$). A bounded central differencing scheme was employed for the convective terms in the momentum equation while the diffusion terms were discretized using pure central differencing. Second-order upwinding was used for all scalars. The temporal terms were discretized using an implicit second-order backward differencing scheme, and a time-step restricting the CFL number to less than 0.5 was chosen. The mesh cell size in the premixer was 0.2 mm or smaller.

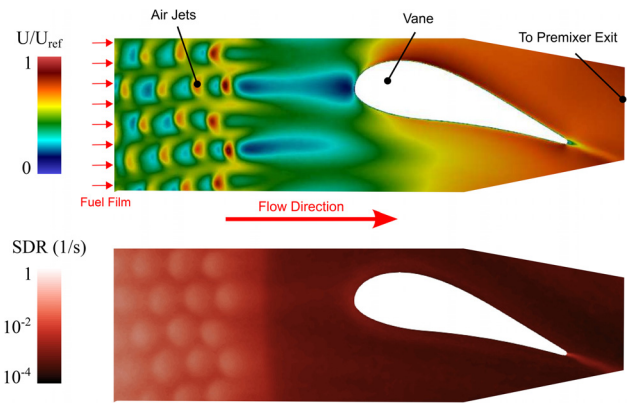

Fig. 1 Normalized mean velocity magnitude field (top) and mean scalar dissipation rate (bottom) in a section of the investigated premixer. For interpretation of the references to colour in the text, the reader is referred to the web version of this article.

The CFD simulation was set at representative full load conditions. These conditions were chosen as the combination of preheat, pressure, and stoichiometry represent a highly reactive operating scenario. In addition, the fuel mixture composition is also of critical importance. In service, the engine is operated with natural gas. However, a gaseous blend of highly reactive dimethyl ether (DME) fuel and less reactive methane (CH_4) is used in this experimental premixer to increase the frequency of AI events [1]. As discussed in Ref. [1], gaseous DME is used to increase the reactivity of methane and thus model the effect that higher hydrocarbons may have on the fuel AI propensity. DME-blended methane is then employed to test the robustness of high-pressure premixers to AI. The CFD simulation considered a fuel mixture of pure CH_4 with 40% (v/v) DME. As explained in Sec. 4, the fuel composition, as well as the temperatures of the air and fuel streams, are modified in the ISR computations, while considering the same underlying mixing field. As the deviations are deemed small enough to cause little differences in velocity and density, the changes in the mixture fraction distribution are negligible.

A detailed CFD analysis on this premixer has already been provided by Jella et al. [1], so only a brief summary is provided here. Figure 1 shows the normalized mean velocity magnitude and mean SDR fields in a section of the premixer, as computed from the non-reacting simulation. The presence of the air jets can be inferred by the red "spots" in the mean velocity field in the upstream region, indicating high velocity. Each red spot is also associated with a wake on the lee side that affects the local residence time and mixing rate. The flow decelerates between the last row of air jets and the guide vane, and is then quickly accelerated on its way to the vane's trailing edge and toward the premixer exit. Until the flow reaches the premixer exit, the mixing intensity is low and the mixture fraction has attained the well-mixed value closely as also indicated by the overall very low SDR values in the downstream region of Fig. 1. Most of the mixing occurs near the fuel injection region where the SDR is very high (not shown). Toward the last rows of air jets, the SDR reaches moderate values but can still span several orders in magnitude depending on the location relative to the air jets, until a significant decay is observed soon after the last row or air jets.

Information regarding the mixing field can also be obtained through the core-averaged mixture fraction PDF, P_η^{**}, which is also directly used in the ISR computations. Figure 2 shows the profile of P_η^{**} as a function of η, i.e., the sample space variable for the mixture fraction, up to a reference mixture fraction, η_0. Two peaks are evident in the PDF profile, one at $\eta = 0$, corresponding to the air stream, and another at the well-mixed mixture fraction, $\bar{\xi}$. In reality, the PDF profile is tri-modal since another peak exists at $\eta = 1$, corresponding to the fuel stream (not shown). The local distribution and the width around $\bar{\xi}$ are a measure of the unmixedness within the premixer. For the same residence time, the higher the PDF at a particular mixture fraction, the lower the local value of the conditional SDR, as inferred by Eq. (9). At the same time, the PDF indicates the extent at which the stoichiometric, ξ_{st}, and the most reactive mixture fractions ξ_{mr} (as defined by Mastorakos [4]) are present in the premixer at both the large and small scales. The most reactive mixture fraction corresponds to the location of the first AI kernel in mixture fraction space in the absence of hydrodynamic stretch. The difference in temperature between the fuel and oxidizer streams inevitably results in variable AI delay times for each mixture fraction, with ξ_{mr} having the most favorable conditions for AI, at least when micromixing effects are not present. Figure 2 shows the dependency of ξ_{st} and ξ_{mr} with increasing level of DME. The premixer's target equivalence ratio is overall fuel-lean with $\bar{\xi}$ being significantly smaller than ξ_{st} and ξ_{mr} for all conditions. It is also evident that up to about 20% (v/v) DME in the fuel, the first AI kernel is more likely to occur in fuel-rich zones, whereas for higher DME levels, AI is more likely in fuel-lean zones. With different operating conditions, ξ_{st} and ξ_{mr} differ but so is the probability of finding these mixture fractions in the premixer. These observations are important for the remainder of the discussion since they can help explain some of the trends observed in the stochastic analysis.

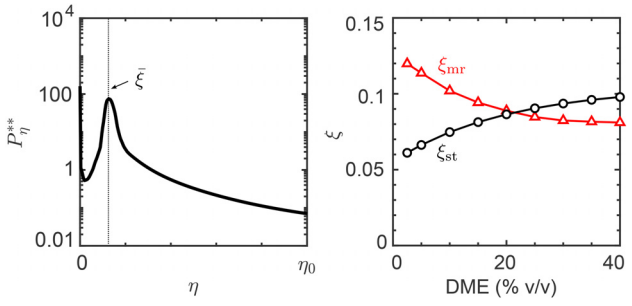

Fig. 2 Core-averaged mixture fraction PDF with well-mixed mixture fraction indicated (left) and dependence of stoichiometric and most reactive mixture fraction to amount of DME in the fuel for the reference temperatures (right)

4 Stochastic Analysis Framework

Once the mixing field from the non-reacting LES simulation is averaged, the ISR approach described in Sec. 2 can then be applied. An ISR network (ISRN) approach can be also applied on the same LES simulation, and results obtained by ISRN in terms of AI propensity and its sensitivity to operating conditions have been presented by Gkantonas et al. [33]. However, the ISR approach guarantees lower computational costs than the ISRN one while maintaining acceptable accuracy, as a close agreement in terms of premixer AI behavior between the two approaches was observed. As this study focuses only on the occurrence, or the absence, of AI inside the premixer, which can be captured by a single ISR, the latter was employed.

The boundary conditions are considered fixed for each ISR simulation. In reality, uncertainties and fluctuations affect the nominal values of the boundary conditions, introducing stochasticity in the output quantities of the premixer. The effect of the random variability of input parameters on the premixer behavior must be predicted and quantified via a stochastic analysis. Figure 3 depicts the general framework of the stochastic analysis adopted in this work. Three random input quantities to the premixer were

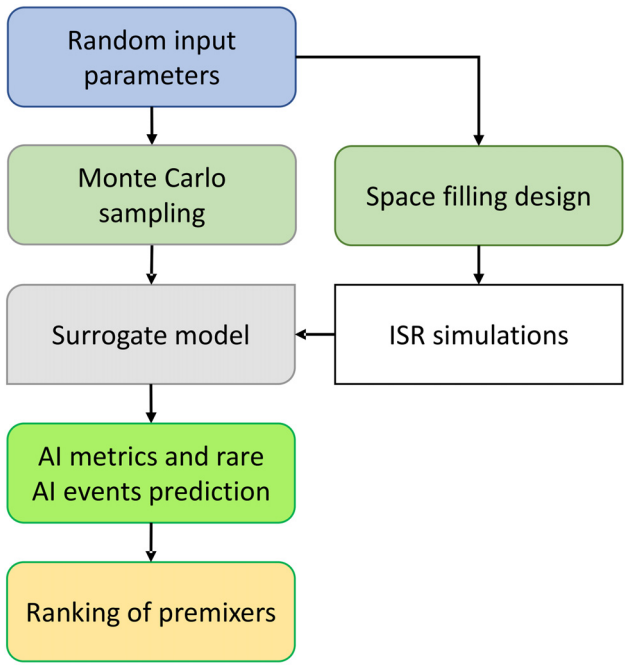

Fig. 3 Methodology scheme

considered, namely, the fuel temperature (T_f), the air temperature (T_{ox}), and the amount of DME (%DME) in the fuel mixture consisting primarily of methane. A space-filling design was generated over the three-dimensional parameter space via the latin hypercube sampling method [51]. For each sampled combination, numerical simulations were performed with the ISR approach. A surrogate model (also called meta-model or response surface) was trained on selected AI metrics obtained as output from the ISR simulations. A brute-force Monte Carlo sampling of the probability density functions (PDFs) of the input parameters was performed and the samples were fed to the surrogate model to obtain the characterization of the distributions of the selected AI metrics. The AI metrics were selected at the premixer exit and correspond to the mass-averaged temperature, T^*_{out}, and the conditional temperature at stoichiometry, $\langle T|\eta_{st}\rangle_{out}$ (η_{st} being the sample space variable of the mixture fraction at stoichiometry, ξ_{st}). They allow to determine if an AI kernel formation event has occurred in the premixer, whereas their probability density function, obtained via Monte Carlo sampling, provides the frequency of AI and hence a quantification of the AI risk.

The methodology described above was slightly modified by the inclusion, prior to the surrogate training step, of a classification method through which the three-dimensional parameter space was clustered in two different subspaces. As a consequence, two separate surrogate models were trained on the corresponding subspaces and achieved higher fitting accuracy than those obtained by only one surrogate model trained on the whole parameter space. Further details are provided in the following section.

5 Results and Discussion

An event can be classified as rare if the frequency of its occurrence is low, or when the overall observational cost is so large that a specific procedure is required to induce it [52]. Although there is no probability level that universally defines a rare event, if we consider a random variable described by a normal distribution, we can say that rare variable outcomes are located at the PDF tails, which require special focus. The aim of this work is to explore the nature of the PDF tails of quantities that can be related to the occurrence of high-temperature AI in a premixer, given a PDF of three input parameters, i.e., T_f, T_{ox}, and %DME in the fuel mixture. Normal distributions were considered for the three parameters, with variable means, representing different operating conditions, and fixed standard deviations σ, equal to 5 K, 10 K, and 2%, for T_f, T_{ox}, and %DME, respectively. For the space-filling design, the ranges of variability of the parameters were set to include the different mean values and their ± 5–6σ uncertainty. A total of 500 different combinations were sampled from the parameter space via LHS, and 500 ISR simulations were performed for each input combination. The simulations took about 5 h to run concurrently over 20 processors. Figures 4 and 5 show the values of T^*_{out} and $\langle T|\eta_{st}\rangle_{out}$ obtained by each ISR simulation. In the figures, T_{ox}, T^*_{out} and $\langle T|\eta_{st}\rangle_{out}$ are normalized by the reference value of T_{ox}, i.e., at the representative full load state, $T_{ox,ref}$, whereas T_f is normalized by the reference value of T_f, $T_{f,ref}$. It can be seen that the two AI metrics correlate with each other since high values of T^*_{out} correspond to high values of $\langle T|\eta_{st}\rangle_{out}$. A more pronounced discontinuity can be noticed in the values of the conditional temperature at stoichiometry at the exit of the premixer, $\langle T|\eta_{st}\rangle_{out}$. Since T^*_{out} is a mass-averaged temperature (see also Eq. (11)), its values are lower than the corresponding ones of $\langle T|\eta_{st}\rangle_{out}$. Hereafter, the results of the methodology described in Sec. 4 will be shown only for one of the two AI metrics, namely, T^*_{out}, as the two quantities strongly correlate with each other and the results obtained for $\langle T|\eta_{st}\rangle_{out}$ would lead to the same discussions and conclusions. The normalized values of $T_{ox}/T_{ox,ref}$, $T_f/T_{f,ref}$ and $T^*_{out}/T_{ox,ref}$ will be reported.

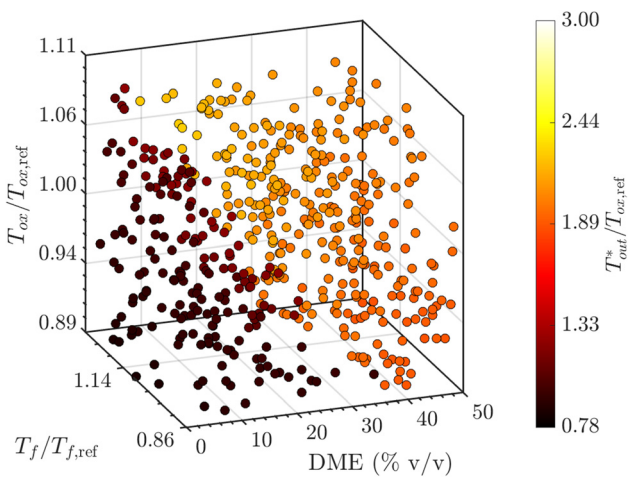

Fig. 4 $T^*_{out}/T_{ox,ref}$ obtained by the 500 ISR simulations

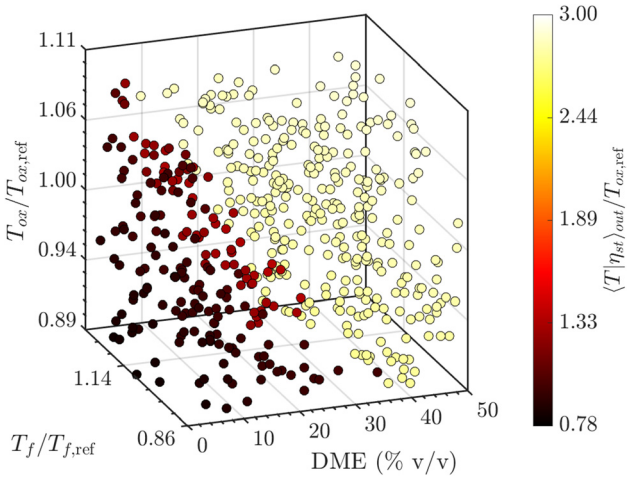

Fig. 5 $\langle T|\eta_{st}\rangle_{out}/T_{ox,ref}$ obtained by the 500 ISR simulations

The training of the surrogate model was attempted for T^*_{out} over the whole parameter space. The accuracy of the surrogate was evaluated during training by 5-fold cross validation. After training, the surrogate fitting errors, i.e., the difference between the values of T^*_{out} provided by the 500 ISR simulation and the corresponding values obtained by the surrogate model, were evaluated. Several surrogate models, such as quadratic and rational-quadratic polynomials, Gaussian processes (GPs), and support-vector machines, were trained in MATLAB on all the 500 T^*_{out} values but none provided acceptable fitting errors (not shown here). It can be seen in Fig. 4 that a sharp discontinuity exists in the set of $T^*_{out}/T_{ox,ref}$ values as there are no values between about 1.33 and 1.89. This can affect the training of response surface and lead to large fitting errors. Thus, a normalized threshold value of $(T^*_{out}/T_{ox,ref})_{tr} = 1.67$ was chosen to distinguish two distinct regions: the subspace of input parameter values at which high-temperature AI does not occur inside the premixer, corresponding to values of $T^*_{out}/T_{ox,ref} \leq 1.67$, and the subspace where AI brings the normalized mass-averaged temperature at the premixer exit above 1.67, namely, $T^*_{out}/T_{ox,ref} > 1.67$. The different behaviors are mostly correlated to the variability of T_{ox} and %DME, while the occurrence of AI seems to be less sensitive to T_f. A classification algorithm, or classifier, can be trained on the ISR responses to automatically distinguish between no-ignition and AI regimes. For each regime, a separate response surface can be constructed to map the stochastic input parameters to the AI metrics. The methodology scheme of Fig. 3 was then modified to include the classification step prior to the training of the surrogate models. In the updated scheme, shown in Fig. 6, the ISR responses are used to train the classifier and the surrogate models. The input parameter

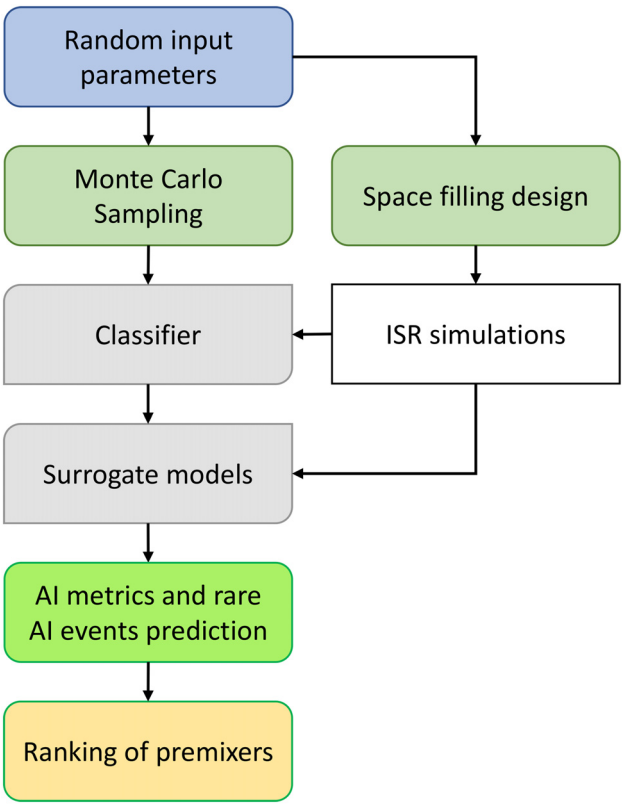

Fig. 6 Methodology scheme modified by the presence of a classification step before the surrogate model training

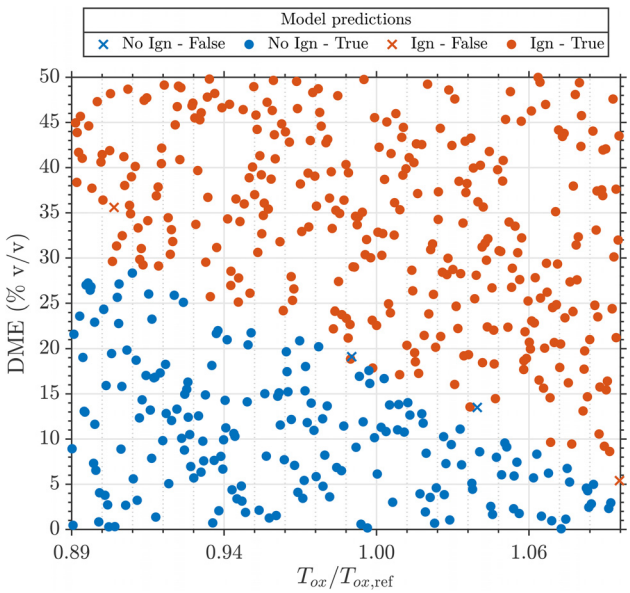

Fig. 7 Classification of T^*_{out}. Two clusters are distinguished by the classifier: the "no ignition" region (blue dots) and the "autoignition" region (red dots). The crosses indicate points that are wrongly assigned by the classifier. For interpretation of the references to colour in this figure legend and in the text, the reader is referred to the web version of this article.

combinations sampled via Monte Carlo are provided to the classifier first, which assigns each combination to either the no-ignition or the AI regime. Based on the assigned regime, the corresponding surrogate model yields the output quantity. Eventually, the characterization of the distributions of the selected AI metrics, and thus a quantification of AI risk, are obtained.

Several classifiers were trained and compared based on their accuracy, which was evaluated via 5-fold cross-validation. The Classification Learner module in MATLAB was used for this task. Logistic Regression provided the highest accuracy (99.2%) in classifying the no-ignition versus AI regimes, as can be seen in Fig. 7, which shows the scatter of the input $T_{\mathrm{ox}}/T_{\mathrm{ox,ref}}$ and %DME values and the separation between the no-ignition region, marked by blue dots, and the AI one, marked by red dots. The crosses indicate the combinations of input values that were wrongly assigned to a certain regime.

After the classification step, two different response surfaces were trained for low T^*_{out} values ($T^*_{\mathrm{out}}/T_{\mathrm{ox,ref}} \leq 1.67$) and high T^*_{out} values ($T^*_{\mathrm{out}}/T_{\mathrm{ox,ref}} > 1.67$). Figure 8 shows the parity plot comparing the low $T^*_{\mathrm{out}}/T_{\mathrm{ox,ref}}$ values obtained by the ISR simulations and those obtained by a GP with Matérn 5/2 kernel (whose mathematical description and details can be found in Ref. [53]) trained in the no-ignition region of the parameter space. Figure 8 also reports the histogram of the surrogate fitting errors, defined as $\delta_T = |T^*_{\mathrm{out,GP}} - T^*_{\mathrm{out,ISR}}|$, where $T^*_{\mathrm{out,GP}}$ and $T^*_{\mathrm{out,ISR}}$ are the values of the mass-averaged exit temperature obtained by the GP and the ISR, respectively. The low-order model is able to predict the low T^*_{out} values with acceptable accuracy as the maximum fitting error is lower than 60 K (corresponding to a relative error lower than 6%). Similarly, Fig. 9 shows the parity plot of the high $T^*_{\mathrm{out}}/T_{\mathrm{ox,ref}}$ values obtained by the ISR simulations and another GP with Matérn 5/2 kernel trained in the AI region of the parameter space. Figure 9 also reports the histogram of the GP fitting errors δ_T previously defined. The low-order model fits the high T^*_{out} values with excellent accuracy as the maximum fitting error is lower than 1 K. The training of the two GPs was performed in less than one minute on a 4-core laptop. The higher accuracy of the GP for high T^*_{out} can be explained by two considerations. First, the number of training points is higher in the AI region of the parameter space since about 62% of the sampled input combinations determine AI in the ISR simulations. A lower number of samples may affect the accuracy of the response surface fitting. Second, the no-ignition region may actually contain ISR simulations where a cool flame exists, characteristic of DME-air combustion (e.g., see Ref. [54] for a recent review on the topic). This may be defined as low-temperature AI. By looking at the parity plot of Fig. 8, sparse data around 1.11 can be noticed, possibly indicating a discontinuity related to the occurrence of low-temperature AI. A third subspace may be identified by considering $T^*_{\mathrm{out}}/T_{\mathrm{ox,ref}}$ lower than 1.67 but higher than 1.11, where another surrogate model may be trained with lower fitting errors. An unsupervised classifier can also be used to distinguish the no-ignition and ignition regions without the need to specify a temperature threshold. Depending on the number of training points, an unsupervised classifier might have a higher accuracy than the classifier used in this work. It might also distinguish the no-ignition region from the low-temperature AI one, where cool flames, characteristic of DME-air combustion, occur. These are open questions that will be addressed in future studies.

The capability of the trained GPs to predict a PDF of T^*_{out} was assessed by considering only one random input quantity, which was described by a hypothetical normal distribution with normalized mean $\mu = 0.99$ and normalized standard deviation $\sigma = 0.01$, i.e., $T_{\mathrm{ox}}/T_{\mathrm{ox,ref}} = \mathcal{N}(0.99, 0.01)$. Additional 45 ISR simulations were performed at fixed %DME = 40 and normalized $T_f/T_{f,\mathrm{ref}} = 0.92$, while $T_{\mathrm{ox}}/T_{\mathrm{ox,ref}}$ was instead varied from 0.93 to 1.05, and provided 45 $T^*_{\mathrm{out}}/T_{\mathrm{ox,ref}}$ values above 1.67. By knowing the correspondence between T_{ox} and T^*_{out} values, a PDF of T^*_{out} can be established a priori. The GP trained for high T^*_{out} must be able to replicate this known PDF. The latter was compared to the one obtained from 10^8 realizations of T^*_{out} provided by the GP queried by as many random samples from the normal distribution of T_{ox}. The 10^8 realizations of T^*_{out} were computed in less than 4 h on a 12-core processor. Excellent agreement was found between the known PDF of T^*_{out} and the one computed by the GP, as shown in Fig. 10, even for very low PDF values, of the order of 10^{-7}. In

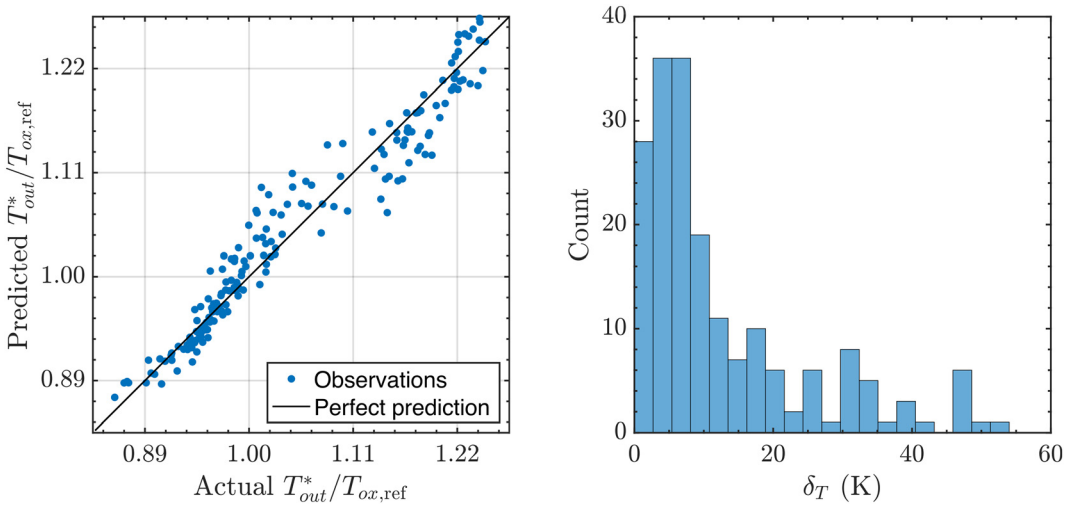

Fig. 8 Parity plot of normalized mass-averaged exit temperatures $T^*_{\mathrm{out}}/T_{\mathrm{ox,ref}} \leq 1.67$ obtained by the ISR simulations and the surrogate model (left) and histogram of the fitting errors of the surrogate model (right)

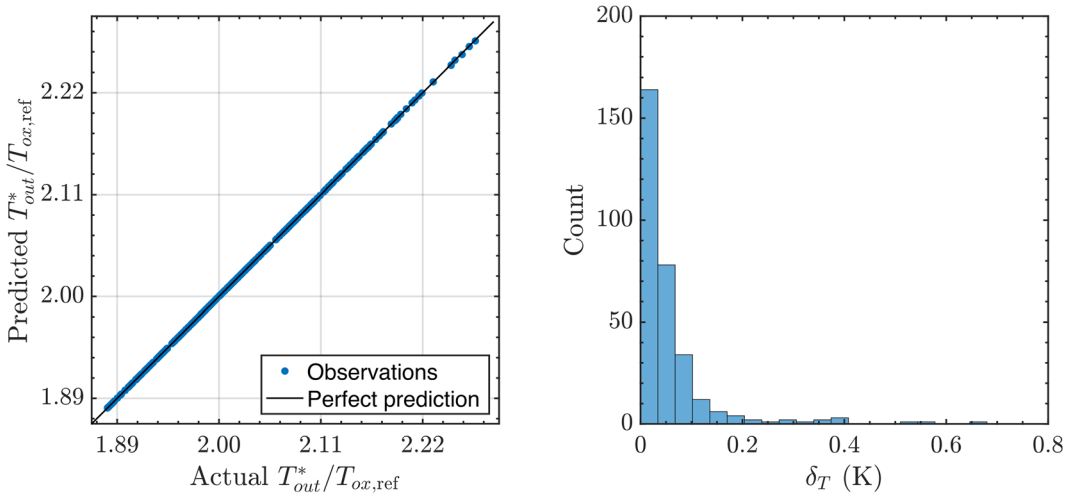

Fig. 9 Parity plot of normalized mass-averaged exit temperatures $T^*_{\mathrm{out}}/T_{\mathrm{ox,ref}} > 1.67$ obtained by the ISR simulations and the surrogate model (left) and histogram of the fitting errors of the surrogate model (right)

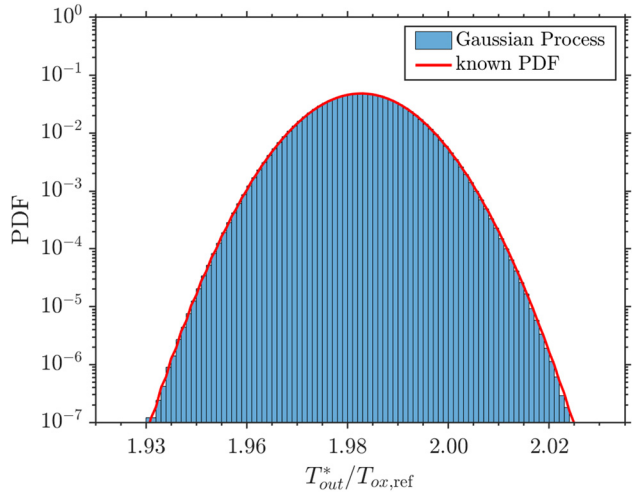

Fig. 10 PDF (in logarithmic scale) of T^*_{out} obtained by the trained Gaussian Process when propagating the uncertainty of only one input quantity, T_{ox}, characterized by a distribution $T_{\mathrm{ox}}/T_{\mathrm{ox,ref}} = \mathcal{N}(0.99, 0.01)$

Fig. 10, the PDF values are related to the non-normalized values of T^*_{out}, although the normalized values of $T^*_{\mathrm{out}}/T_{\mathrm{ox,ref}}$ are reported. This result confirms the accuracy of the GP, even for additional data points that were not used for the training of the GP itself, and validates the use of a response surface for fast estimation of an AI metric.

At the Monte Carlo sampling stage, normal distributions are assumed for T_f, T_{ox}, and %DME, having (non-normalized) standard deviations $\sigma_{T_f} = 5\,\mathrm{K}$, $\sigma_{T_{\mathrm{ox}}} = 10\,\mathrm{K}$, and $\sigma_{\%\mathrm{DME}} = 2$, respectively. First, the following mean values are considered for the input distributions: $\mu_{T_f} = 0.92\,T_{f,\mathrm{ref}}$, $\mu_{T_{\mathrm{ox}}} = 0.99\,T_{\mathrm{ox,ref}}$, and $\mu_{\%\mathrm{DME}} = 20$. A total of 10^7 random samples of the normal PDFs were provided to the classifier and assigned to the corresponding subspaces where T^*_{out} was computed by the related surrogate model. Figure 11 shows the obtained scatter of $T^*_{\mathrm{out}}/T_{\mathrm{ox,ref}}$ values, along with the output of the ISR simulations. The ISR values of $T^*_{\mathrm{out}}/T_{\mathrm{ox,ref}}$ are indicated by filled circles, whereas the 10^7 surrogate realizations of $T^*_{\mathrm{out}}/T_{\mathrm{ox,ref}}$ are marked by empty circles. A PDF of the non-normalized T^*_{out} values was then obtained and is also shown in Fig. 11. The probability of $T^*_{\mathrm{out}} > T^*_{\mathrm{out,tr}}$, with $T^*_{\mathrm{out,tr}} = 1.67\,T_{\mathrm{ox,ref}}$, can be seen as the AI probability in the premixer at the considered nominal (mean) values of the input quantities and is given by $P_{\mathrm{AI}} = \int_{T^*_{\mathrm{out,tr}}}^{\infty} P(T^*_{\mathrm{out}})\,dT^*_{\mathrm{out}}$. At these

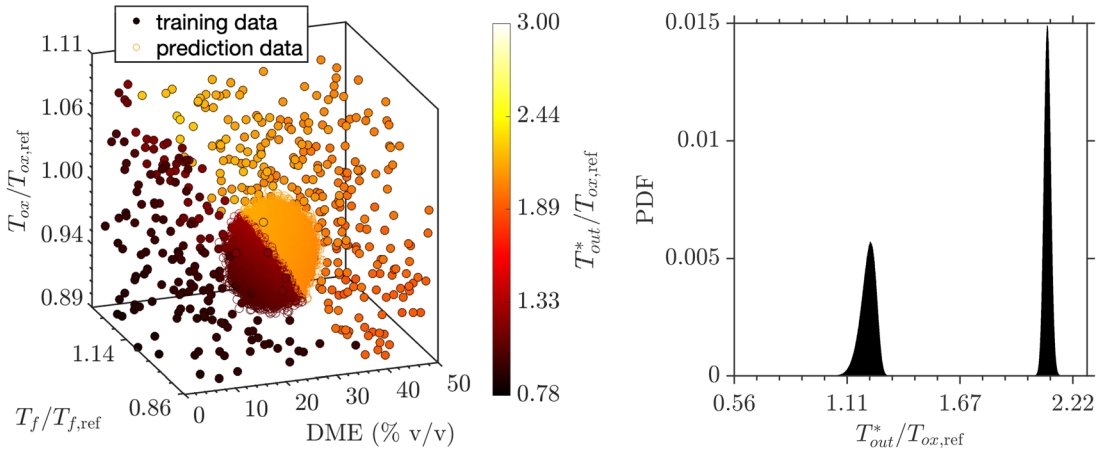

Fig. 11 (Left) $T^*_{out}/T_{ox,ref}$ obtained by the 500 ISR runs (filled circles) and the 10^7 realizations of the surrogate models (open circles). (Right) PDF of T^*_{out} computed by the surrogate models.

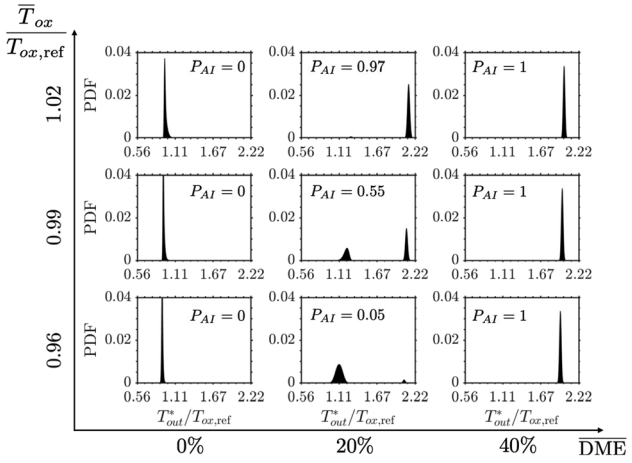

Fig. 12 PDFs of T^*_{out} at different mean values of T_{ox} and %DME and corresponding autoignition probabilities P_{AI}

conditions, the probability that AI would occur in the premixer is about 54.6%.

Different mean values of T_f, T_{ox}, and %DME can be considered, while keeping constant their standard deviations. Since the fuel temperature appears to have the lowest influence on the onset of AI in the premixer, the AI risk was quantified at different mean value pairs of T_{ox} and %DME, while keeping $T_f/T_{f,ref}=0.92$ fixed. Figure 12 shows the probability distributions of T^*_{out} obtained at normalized $\mu_{T_{ox}}/T_{ox,ref}\equiv\bar{T}_{ox}/T_{ox,ref}=0.96$, 0.99, 1.02, and $\mu_{\%DME}=0$, 20, 40. When $\mu_{\%DME}=0$, the volumetric amount of DME in the fuel mixture cannot be negative, hence a half-normal PDF of %DME was considered for the positive values of %DME. Once again, 10^7 random combinations were sampled for each case. It can been seen from Fig. 12 that AI never occurs for the lowest amounts of DME in the fuel mixture as increasing the air temperature does not change the premixer behavior. When the mean volumetric amount of DME is equal to 20%, AI occurs 5% of the time at $\mu_{T_{ox}}/T_{ox,ref}=0.96$, and increasing the air temperature determines a higher probability of AI, up to 97% at $\mu_{T_{ox}}/T_{ox,ref}=1.02$. Finally, when the mean volumetric amount of DME is 40%, AI occurs at all the considered mean air temperatures.

In order to capture rare AI events, the analysis described above was repeated for another set of mean values, i.e., $\mu_{T_f}/T_{f,ref}=0.95$, $\mu_{T_{ox}}/T_{ox,ref}=1.03$, and $\mu_{\%DME}=3$. Since computing a probability of order 10^{-6} with 90% accuracy requires around 10^8 realizations [52], as many random samples were taken and fed to the classifier and the surrogate models. Samples with negative values of %DME were disregarded during the process. The resulting values of $T^*_{out}/T_{ox,ref}$ are shown in Fig. 13, which also illustrates the position of the sampled region in the parameter space. The cloud of sampled points barely crosses the AI subspace, indicating AI may occur in the premixer at these conditions. The resulting PDF of

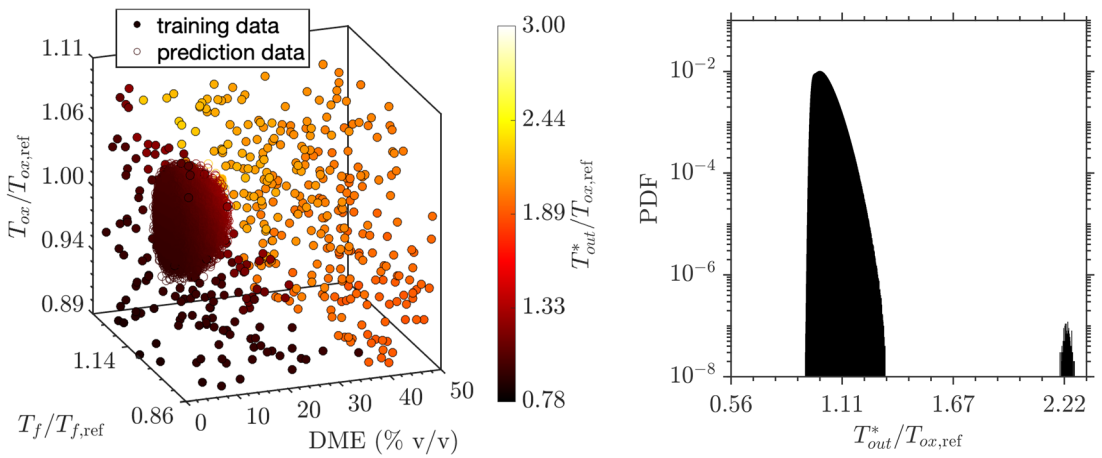

Fig. 13 (Left) $T^*_{out}/T_{ox,ref}$ obtained by the 500 ISR runs (filled circles) and the 10^8 realizations of the surrogate models (open circles). (Right) PDF (in logarithmic scale) of T^*_{out} computed by the surrogate models.

T^*_{out} is also shown in Fig. 13 (note that the vertical axis is logarithmic) and confirms the occurrence of rare AI events bringing $T^*_{out}/T_{ox,ref}$ up to around 2.22. At these conditions, the probability that AI would occur in the premixer was calculated as previously described and is equal to $P_{AI} = 2.8 \times 10^{-6}$.

6 Summary and Conclusions

A novel approach using ISR postprocessing on a non-reacting CFD solution and surrogate modeling for stochastic estimation of nonpremixed autoignition in a aero-derivative premixer has been presented. The variability of three influential input parameters, i.e., fuel temperature, air temperature, and volume fraction of dimethyl ether (DME) in the fuel mixture, was propagated to estimate the distributions of physical quantities labeled as AI metrics, as they can indicate the occurrence of high-temperature AI inside the premixer. In this work, the mass-averaged temperature at the premixer exit was chosen as the target AI metric.

A total of 500 ISR simulations of the premixer were first performed at input parameter combinations sampled via a space-filling design. The obtained estimations of the mass-averaged temperature at the premixer exit revealed the presence of two distinct regions of the three-dimensional parameter space, which hindered the training of a single surrogate model for the chosen AI metric. Thus, a classification step was introduced before the response surface training to distinguish the no-ignition and AI regions. The classifier was trained on the already performed 500 ISR simulations. On each subregion of the parameter space identified by the classifier, an accurate surrogate model was then trained for the AI metric on the same ISR simulations. The probability distribution of the mass-averaged exit temperature was then computed by propagating the variability of the input parameters via Monte Carlo sampling. The classifier assigned each random sample to the correct subspace, where the corresponding surrogate model mapped the input parameters to the AI metric. The AI probability was then estimated at several nominal values of the input quantities by integrating the obtained probability density functions of the mass-averaged exit temperature.

In order to obtain a reliable estimate of probabilities of rare events, such as AI in an aero-derivative premixer, a large number of realizations is necessary. For Monte Carlo methods, computing a probability of order 10^{-6} with 90% accuracy requires around 10^8 realizations. Intense research focused on mitigating this issue, leading to variance reduction methods for unbiased probability estimators. The issue is alleviated here by employing response surfaces that can provide 10^8 realizations at much reduced computational costs with limited loss of accuracy. Moreover, the training of accurate response surfaces may require a significant number of CFD simulations, up to a point where using response surfaces does not reduce any computational effort. This risk is mitigated by using an ISR approach which combines detailed chemistry with average flow and mixing fields obtained from one inert CFD simulation, thus keeping the computational cost at the lowest.

In this methodology, the accuracy of the AI risk quantification is strongly related to the efficiency of the classification method. The frontier that separates the no ignition and the AI regions must be predicted by the classifier correctly. Other classification algorithms, in a supervised or unsupervised fashion, can be employed to achieve higher accuracy. Moreover, instead of single ISR runs, simulations employing a network of ISRs, i.e., the ISRN approach, can be leveraged to improve the characterization of the border between the subspaces with a moderate computational penalty. The accuracy of a classifier, trained on both ISR and ISRN simulations, will benefit from the enhanced characterization of the frontier manifold. Nonetheless, the methodology presented in this work has shown its capability to quantify the AI risk in an efficient and computationally feasible way. Small fluctuations of input parameters can cause significant changes in the premixer output response, and simple physics-based tools that combine chemical reaction and mixing effects, such as the ISR approach, can be reliably used to study the premixer robustness to AI risk. AI is expected to become more important in the future with a transition from conventional to next-generation fuels. Hence, it is very important to characterize the input uncertainties (e.g., in terms of a mean and a variance) and to be aware of the tails of the distributions (e.g., at ± 6 standard deviations), so that premixer systems can be evaluated at these remote (typically off-design) conditions. Based on the AI risk, different premixers can be ranked, and the best premixer design and operating conditions can be selected for its intended use. The use of this joint ISR(N)-classifier-surrogate approach for premixer design optimization for rare AI events are expected in future works.

Funding Data

- Siemens Energy (Funder ID: 10.13039/501100015664).

References

[1] Jella, S., Bourque, G., Gauthier, P., Versailles, P., Bergthorson, J., Park, J.-W., Lu, T., Panigrahy, S., and Curran, H., 2021, "Analysis of Auto-Ignition Chemistry in Aeroderivative Premixers at Engine Conditions," ASME J. Eng. Gas Turbines Power, **143**(11), p. 111024.

[2] Mastorakos, E., Baritaud, T., and Poinsot, T., 1997, "Numerical Simulations of Autoignition in Turbulent Mixing Flows," Combust. Flame, **109**(1–2), pp. 198–223.

[3] Markides, C., and Mastorakos, E., 2005, "An Experimental Study of Hydrogen Autoignition in a Turbulent co-Flow of Heated Air," Proc. Combust. Inst., **30**(1), pp. 883–891.

[4] Mastorakos, E., 2009, "Ignition of Turbulent Non-Premixed Flames," Prog. Energy Combust. Sci., **35**(1), pp. 57–97.

[5] Xiouris, C., Ye, T., Jayachandran, J., and Egolfopoulos, F., 2016, "Laminar Flame Speeds Under Engine-Relevant Conditions: Uncertainty Quantification and Minimization in Spherically Expanding Flame Experiments," Combust. Flame, **163**, pp. 270–283.

[6] Zhang, Y., Jeanson, M., Mével, R., Chen, Z., and Chaumeix, N., 2021, "Tailored Mixture Properties for Accurate Laminar Flame Speed Measurement From Spherically Expanding Flames: Application to h2/o2/n2/he Mixtures," Combust. Flame, **231**, p. 111487.

[7] Prager, J., Najm, H., Sargsyan, K., Safta, C., and Pitz, W., 2013, "Uncertainty Quantification of Reaction Mechanisms Accounting for Correlations Introduced by Rate Rules and Fitted Arrhenius Parameters," Combust. Flame, **160**(9), pp. 1583–1593.

[8] Ji, W., Wang, J., Zahm, O., Marzouk, Y., Yang, B., Ren, Z., and Law, C., 2018, "Shared Low-Dimensional Subspaces for Propagating Kinetic Uncertainty to Multiple Outputs," Combust. Flame, **190**, pp. 146–157.

[9] Lipardi, A., Versailles, P., Watson, G., Bourque, G., and Bergthorson, J., 2017, "Experimental and Numerical Study on Nox Formation in ch4–Air Mixtures Diluted With Exhaust Gas Components," Combust. Flame, **179**, pp. 325–337.

[10] Yousefian, S., Bourque, G., and Monaghan, R., 2019, "Uncertainty Quantification of NOx and CO Emissions in a Swirl-Stabilized Burner," ASME J. Eng. Gas Turbines Power, **141**(10), p. 101014.

[11] Iavarone, S., Bertolino, A., Cafiero, M., and Parente, A., 2022, "Combined Effect of Experimental and Kinetic Uncertainties on No Predictions in Low-Pressure Premixed Laminar h2/ch4/co-Air and h2/ch4/co/c6h6-Air Flames," Fuel, **320**, p. 123800.

[12] Oh, M.-S., and Berger, J., 1992, "Adaptive Importance Sampling in Monte Carlo Integration," J. Stat. Comput. Simul., **41**(3–4), pp. 143–168.

[13] Wouters, J., and Bouchet, F., 2016, "Rare Event Computation in Deterministic Chaotic Systems Using Genealogical Particle Analysis," J. Phys. A: Math. Theory, **49**(37), p. 374002.

[14] Bouchet, F., Rolland, J., and Wouters, J., 2019, "Rare Event Sampling Methods," Chaos: Interdiscip. J. Nonlinear Sci., **29**(8), p. 080402.

[15] Ziehn, T., and Tomlin, A. S., 2008, "A Global Sensitivity Study of Sulfur Chemistry in a Premixed Methane Flame Model Using Hdmr," Int. J. Chem. Kinetics, **40**(11), pp. 742–753.

[16] Najm, H. N., 2009, "Uncertainty Quantification and Polynomial Chaos Techniques in Computational Fluid Dynamics," Annu. Rev. Fluid Mech., **41**(1), pp. 35–52.

[17] Iavarone, S., Oreluk, J., Smith, S., Hegde, A., Li, W., Packard, A., Frenklach, M., Smith, P., Contino, F., and Parente, A., 2018, "Application of Bound-to-Bound Data Collaboration Approach for Development and Uncertainty Quantification of a Reduced Char Combustion Model," Fuel, **232**, pp. 769–779.

[18] Yousefian, S., Bourque, G., and Monaghan, R., 2021, "Bayesian Inference and Uncertainty Quantification for Hydrogen-Enriched and Lean-Premixed Combustion Systems," Int. J. Hydrogen Energy, **46**(46), pp. 23927–23942.

[19] Yousefian, S., Bourque, G., and Monaghan, R., 2017, "Review of Hybrid Emissions Prediction Tools and Uncertainty Quantification Methods for Gas Turbine Combustion Systems," ASME Paper No. GT2017-64271.

[20] Smith, N., 1994, "Development of the Conditional Moment Closure Method for Modelling Turbulent Combustion," Ph.D. thesis, University of Sydney, Sydney, Australia.

[21] Mobini, K., 1998, "An investigation of the Imperfectly Stirred Reactor Modelling of Recirculating Combustion Flows," Ph.D. thesis, University of Sydney, Sydney, Australia.
[22] Mobini, K., and Bilger, R., 2004, "Imperfectly Stirred Reactor Model Predictions of Reaction in a Burner With Strong Recirculation," Combust. Sci. Technol., **176**(1), pp. 45–70.
[23] Mobini, K., and Bilger, R., 2009, "Parametric Study of the Incompletely Stirred Reactor Modeling," Combust. Flame, **156**(9), pp. 1818–1827.
[24] Klimenko, A., and Bilger, R., 1999, "Conditional Moment Closure for Turbulent Combustion," Prog. Energy Combustion Science, **25**(6), pp. 595–687.
[25] Gough, A., Mobini, K., Chen, Y., and Bilger, R., 1998, "Measurements and Predictions in a Confined Bluff-Body Burner Modeled as an Imperfectly Stirred Reactor," Proc. Combust. Inst., **27**(2), pp. 3181–3188.
[26] Trivedi, S., Gkantonas, S., Wright, Y., Parravicini, M., Barro, C., and Mastorakos, E., 2021, "Conditional Moment Closure Approaches for Simulating Soot and NOx in a Heavy-Duty Diesel Engine," SAE Paper No. 2021-24-0041.
[27] Gkantonas, S., Giusti, A., and Mastorakos, E., 2019, "Incompletely Stirred Reactor Network Modelling for Soot Emissions Prediction in Aero-Engine Combustors," Proceedings of the International Workshop on Clean Combustion: Principles and Applications, Darmstadt, Germany, Sept. 25–26.
[28] Gkantonas, S., Giusti, A., and Mastorakos, E., 2020, "Incompletely Stirred Reactor Network Modeling of a Model Gas Turbine Combustor," AIAA Paper No. 2020-2087.
[29] Gkantonas, S., Foale, J., Giusti, A., and Mastorakos, E., 2020, "Soot Emission Simulations of a Single Sector Model Combustor Using Incompletely Stirred Reactor Network Modeling," ASME J. Eng. Gas Turbines Power, **142**(10), p. 101007.
[30] Gkantonas, S., 2021, "Predicting Soot Emissions with Advanced Turbulent Reacting Flow Modelling," Ph.D. thesis, University of Cambridge, Cambridge, UK.
[31] Iavarone, S., Gkantonas, S., and Mastorakos, E., 2022, "Incompletely Stirred Reactor Network Modeling for the Estimation of Turbulent Non-Premixed Autoignition," 28th International Colloquium on the Dynamics of Explosions and Reactive Systems (ICDERS), Naples, Italy, June 19–24, Paper No. 51.
[32] Iavarone, S., Gkantonas, S., and Mastorakos, E., 2022, "Stochastic Low-Order Modelling of Hydrogen Autoignition in a Turbulent Non-Premixed Flow," Proceedings of the Combustion Institute, **39**.
[33] Gkantonas, S., Jella, S., Iavarone, S., Versailles, P., Mastorakos, E., and Bourque, G., 2022, "Estimations of Autoignition Propensity in Aeroderivative Gas Turbine Premixers Using Incompletely Stirred Reactor Network Modelling," ASME J. Eng. Gas Turbines Power, **144**(10), p. 101009.
[34] Jones, W., and Navarro-Martinez, S., 2008, "Study of Hydrogen Auto-Ignition in a Turbulent Air co-Flow Using a Large Eddy Simulation Approach," Comput. Fluids, **37**(7), pp. 802–808.
[35] Stanković, I., Triantafyllidis, A., Mastorakos, E., Lacor, C., and Merci, B., 2011, "Simulation of Hydrogen Auto-Ignition in a Turbulent co-Flow of Heated Air With LES and CMC Approach," Flow, Turbul. Combust., **86**(3–4), pp. 689–710.
[36] Navarro-Martinez, S., and Kronenburg, A., 2011, "Flame Stabilization Mechanisms in Lifted Flames," Flow, Turbul. Combust., **87**(2–3), pp. 377–406.
[37] Buckrell, A. J. M., and Devaud, C. B., 2013, "Investigation of Mixing Models and Conditional Moment Closure Applied to Autoignition of Hydrogen Jets," Flow, Turbul. Combust., **90**(3), pp. 621–644.
[38] Chen, J.-Y., 1997, "Stochastic Modeling of Partially Stirred Reactors," Combust. Sci. Technol., **122**(1–6), pp. 63–94.
[39] Peters, N., 1984, "Laminar Diffusion Flamelet Models in Non-Premixed Turbulent Combustion," Prog. Energy Combust. Sci., **10**(3), pp. 319–339.
[40] Mortensen, M., 2005, "Consistent Modeling of Scalar Mixing for Presumed, Multiple Parameter Probability Density Functions," Phys. Fluids, **17**(1), p. 018106.
[41] Devaud, C. B., Bilger, R. W., and Liu, T., 2004, "A New Method of Modeling the Conditional Scalar Dissipation Rate," Phys. Fluids, **16**(6), pp. 2004–2011.
[42] Brown, P., and Hindmarsh, A., 1989, "Reduced Storage Matrix Methods in Stiff ODE Systems," Appl. Math. Comput., **31**, pp. 40–91.
[43] O'Brien, E., and Jiang, T., 1991, "The Conditional Dissipation Rate of an Initially Binary Scalar in Homogeneous Turbulence," Phys. Fluids A: Fluid Dyn., **3**(12), pp. 3121–3123.
[44] Wright, Y., Depaola, G., Boulouchos, K., and Mastorakos, E., 2005, "Simulations of Spray Autoignition and Flame Establishment With Two-Dimensional CMC," Combust. Flame, **143**(4), pp. 402–419.
[45] Scarinci, T., Freeman, C., and Day, I., 2004, "Passive Control of Combustion Instability in a Low Emissions Aeroderivative Gas Turbine," ASME Paper No. GT2004-53767.
[46] Nicoud, F., and Ducros, F., 1999, "Subgrid-Scale Stress Modelling Based on the Square of the Velocity Gradient Tensor," Flow, Turbul. Combust., **62**(3), pp. 183–200.
[47] Jiménez, C., Ducros, F., Cuenot, B., and Bédat, B., 2001, "Subgrid Scale Variance and Dissipation of a Scalar Field in Large Eddy Simulations," Phys. Fluids, **13**(6), pp. 1748–1754.
[48] Branley, N., and Jones, W., 2001, "Large Eddy Simulation of a Turbulent Non-Premixed Flame," Combust. Flame, **127**(1–2), pp. 1914–1934.
[49] Garmory, A., and Mastorakos, E., 2011, "Capturing Localised Extinction in Sandia Flame F With LES-CMC," Proc. Combust. Inst., **33**(1), pp. 1673–1680.
[50] Sitte, M. P., Turquand d'Auzay, C., Giusti, A., Mastorakos, E., and Chakraborty, N., 2020, "A-Priori Validation of Scalar Dissipation Rate Models for Turbulent Non-Premixed Flames," Flow, Turbul. Combust., **107**(1), pp. 201–218.
[51] McKay, M. D., Beckman, R. J., and Conover, W. J., 1979, "Comparison of Three Methods for Selecting Values of Input Variables in the Analysis of Output From a Computer Code," Technometrics, **21**(2), pp. 239–245.
[52] Hassanaly, M., and Raman, V., 2021, "Classification and Computation of Extreme Events in Turbulent Combustion," Prog. Energy Combust. Sci., **87**, p. 100955.
[53] Rasmussen, C., and Williams, C., 2005, *Gaussian Processes for Machine Learning*, The MIT Press, Cambridge, MA.
[54] Ju, Y., Reuter, C., Yehia, O., Farouk, T., and Won, S., 2019, "Dynamics of Cool Flames," Prog. Energy Combust. Sci., **75**, p. 100787.